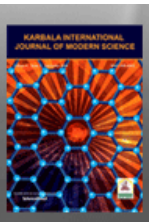

Karbala International Journal of Modern Science

Volume 12 | Issue 1 Article 5

Chaos Engineering in Multi-Gigahertz Solid-State Lasers: A Novel Approach to Optoelectronic Control

Mikhail V. Gorbunkov
P.N. Lebedev Physical Institute of the Russian Academy of Sciences, Moscow, Russian Federation,
gorbunkovmv@lebedev.ru

Yulia Ya. Maslova
P.N. Lebedev Physical Institute of the Russian Academy of Sciences, Moscow, Russian Federation

Yulia A. Sinichkina
P.N. Lebedev Physical Institute of the Russian Academy of Sciences, Moscow, Russian Federation,
sinichkina_y@mail.ru

Chaos Engineering in Multi-Gigahertz Solid-State Lasers: A Novel Approach to Optoelectronic Control

Abstract

This paper presents a comprehensive study of a multi-gigahertz chaotic generator of light pulses based on solid-state laser sources, including fiber lasers, governed by carefully designed positive and negative feedback loops. It harnesses the inherent nonlinear dynamics within a solid-state laser controlled by a combination of two inertial feedback loops, enabling the realization of complex chaotic behavior, including the logistic map scenario, under moderate amplification conditions. The laser system dynamics are rigorously investigated through theoretical modeling, employing a nonlinear map approach, and high-resolution picosecond simulations. The results of our numerical simulations highlight the efficacy of fast electro-optical feedback system with adjustable delays and relative loop sensitivity, providing valuable insights into the design and optimization of chaotic light pulse generators for diverse applications, including secure communication and advanced signal processing. The control scheme integrating Self-Starting Harmonic Mode-Locking (SSHML) for generation of multiple short pulses inside the laser resonator incorporates a memory-erasure regime that reduces the response time by eliminating interference from neighboring pulses. Our study focuses on the features of the electro-optic modulation process. We demonstrate that variation of bias voltage significantly influences the required overall gain for nonlinear dynamics onset. We examined the reversal of the bias voltage polarity and found that selecting a zero value is sufficient to significantly reduce the operating gain. Corresponding requirements for the photodiodes of the control system have been defined. As a result, recommendations for selecting optimal control conditions have been developed. Our findings facilitate easier experimental realization of the chaotic generator.

Keywords

optoelectronic feedback; solid-state laser; deterministic chaos

RESEARCH PAPER

Chaos Engineering in Multi-gigahertz Solid-state Lasers: A Novel Approach to Optoelectronic Control

Mikhail V. Gorbunkov, Yulia Y. Maslova, Yulia A. Sinichkina*

P.N. Lebedev Physical Institute of the Russian Academy of Sciences, Moscow, Russian Federation

Abstract

This paper presents a comprehensive study of a multi-gigahertz chaotic generator of light pulses based on solid-state laser sources, including fiber lasers, governed by carefully designed positive and negative feedback loops. It harnesses the inherent nonlinear dynamics within a solid-state laser controlled by a combination of two inertial feedback loops, enabling the realization of complex chaotic behavior, including the logistic map scenario, under moderate amplification conditions. The laser system dynamics are rigorously investigated through theoretical modeling, employing a nonlinear map approach, and high-resolution picosecond simulations. The results of our numerical simulations highlight the efficacy of fast electro-optical feedback system with adjustable delays and relative loop sensitivity, providing valuable insights into the design and optimization of chaotic light pulse generators for diverse applications, including secure communication and advanced signal processing. The control scheme integrating Self-Starting Harmonic Mode-Locking (SSHML) for generation of multiple short pulses inside the laser resonator incorporates a memory-erasure regime that reduces the response time by eliminating interference from neighboring pulses. Our study focuses on the features of the electro-optic modulation process. We demonstrate that variation of bias voltage significantly influences the required overall gain for nonlinear dynamics onset. We examined the reversal of the bias voltage polarity and found that selecting a zero value is sufficient to significantly reduce the operating gain. Corresponding requirements for the photodiodes of the control system have been defined. As a result, recommendations for selecting optimal control conditions have been developed. Our findings facilitate easier experimental realization of the chaotic generator.

Keywords: Optoelectronic feedback, Solid-state laser, Deterministic chaos

1. Introduction

It is known that nonlinear optical systems with feedback can exhibit complex dynamic regimes, such as periodic oscillations, self-pulsations, and optical chaos [1]. Optical instabilities can also arise in laser systems [2,3]. Delayed feedback under certain conditions leads to regular and chaotic self-oscillatory regimes [4].

Experimental investigations of chaotic pathways in semiconductor lasers with external optical feedback are detailed in Ref. [5]. Experiments with semiconductor lasers revealed that exceeding the chaos threshold by 30 % leads to system uncontrollability, even with adaptive algorithms [6,7]. Intentional generation of chaotic regimes is also relevant for optical systems [8,9]. Systems with controlled chaotic dynamics are increasingly applied across scientific and technical fields. Interest in chaotic light generators extends to biology and medicine [10]. Chaotic signals can enhance data transmission security, e.g., in chaotic masking schemes where information is embedded in chaotic carriers [11]. Emerging methods for broadband communication systems demand fast, simple, and reliable chaotic light pulse generators [12–15].

A promising approach for chaotic generators involves diode-pumped solid-state lasers controlled by inertial optoelectronic feedback loops. While purely inertial feedback tends to limit nonlinear

Received 15 August 2025; revised 17 November 2025; accepted 20 November 2025.
Available online 22 December 2025

* Corresponding author.
E-mail addresses: gorbunkovmv@lebedev.ru (M.V. Gorbunkov), jmaslova@mail.ru (Y.Y. Maslova), sinichkina_y@mail.ru (Y.A. Sinichkina).

https://doi.org/10.33640/2405-609X.3440

dynamics [16], the method of memory erasure—implemented via a secondary positive feedback loop—enables rich, logistic-map-like behavior and significantly expands the variety of achievable nonlinear regimes. This approach effectively truncates the infinite sum in the nonlinear map describing the system, and with proper selection of the relative sensitivity coefficient, the dynamics can be decomposed into independent mappings for each pulse circulating in the resonator. This principle also facilitates the combination of memory erasure with self-mode-locking, supporting tens of short pulses in the resonator and thereby enabling multi-gigahertz repetition rates [17].

Our group has systematically developed this technical foundation. We first established Self-Starting Harmonic Mode-Locking (SSHML) using a single delayed negative feedback loop, which generates m equidistant pulses per round-trip and provides analytical tools for predicting pulse duration and stability [18]. This was advanced in Ref. [19] by combining SSHML with RF modulation to create a versatile picosecond master oscillator synchronized to accelerator frequencies. Most recently, [17] demonstrated that introducing a secondary positive feedback loop for memory erasure induces complex nonlinear dynamics, including period-doubling cascades and deterministic chaos, at multi-gigahertz rates.

However, these pioneering studies [16,17] revealed a major obstacle to practical implementation: the threshold gain for chaos was prohibitively high, exceeding that of the logistic map and limiting the maximum acceptable amplification. The present work directly addresses this critical issue. We conduct a thorough investigation of the nonlinear dynamics threshold in relation to key optoelectronic feedback parameters, with a particular focus on optimizing the modulator bias voltage. Our results demonstrate a pathway to drastically lower the required gain, thereby representing a crucial step toward the realization of compact, energy-efficient chaotic light sources.

2. Electro-optical control and corresponding nonlinear map

Let us consider a laser with control based on a two-section electro-optic modulator, intracavity polarizer and variable delay feedback. The electrodes are controlled by two optoelectronic circuits (Fig. 1) and have a common bias voltage U_0. The capacitances of the photodiode's storage capacitor C_s, the bias capacitor C_b and the modulator crystal C satisfy the inequality $C_s>>C_b>>C$.

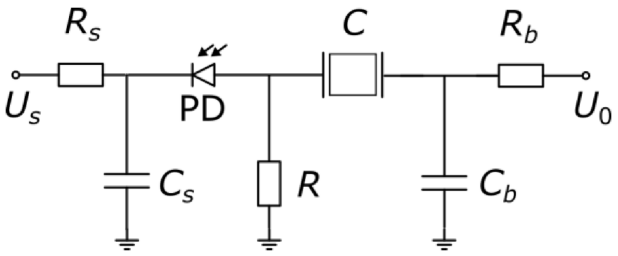

Fig. 1. Schematic diagram of electro-optic modulator. PD is the photodiode, R_s and R_b are resistors, C modulator crystal capacitance, C_s, C_b capacities, U_s, U_0 voltages; subscript 's' denotes the charge storage circuit and 'b' denotes the bias voltage supply circuit.

The electro-optic modulator's transmission is determined by the sum of U_0 and the sum of signals from the photodiodes. Photodiode current is calculated as the convolution of the pulse intensity that hits photodiode with the response function taking into account feedback loop sensitivity and optical delay.

The control circuits for the modulator sections incorporate a photodiode as a current source, and thus the control voltages $U_1(t)$ and $U_2(t)$ applied to the electro-optic crystals are calculated from differential equations

$$\frac{dU_1(t)}{dt}+\frac{U_1(t)}{R_1C_1}=\frac{i_{d1}(t)}{C_1}, \tag{1}$$

$$\frac{dU_2(t)}{dt}+\frac{U_2(t)}{R_2C_2}=\frac{i_{d2}(t)}{C_2}, \tag{2}$$

where $i_{d1,2}$ are photodiode currents and R_1C_1, R_2C_2 are time constants of control circuits. In this work, we assume $R_1 = R_2$ and $C_1 = C_2$.

The transmission function P of the two-section electro-optic modulator, given by $P = \cos^2((u_1 + u_2 + u_0)\pi/2)$ is shown in Fig. 2 where it is plotted versus $u = u_1 + u_2$ normalized by half-wave voltage $u_{\lambda/2}$. This normalization is used below

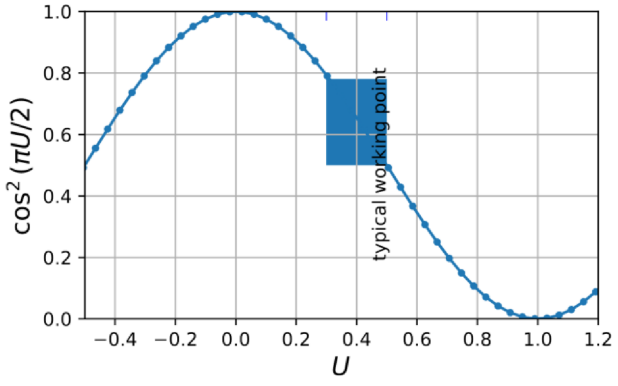

Fig. 2. Electro-optic modulator transmission versus the control signal in the units of half-wave voltage $u_{\lambda/2}$.

in the subsequent analysis. Thus, if we consider such a device as an element of intracavity control, then the incident light is the light taken from the laser resonator and feedback action is achieved. When the goal is to stabilize the pulse amplitude, typical values of u_0 are chosen to be in the range of (0.3–0.5) for negative feedback to be linear with maximum.

A laser, in the general case implementing the proposed control scenario of generating light pulses with a multi-gigahertz repetition rate and chaotic amplitude distribution, contains: a resonator, an active medium, an electro-optic modulator for synchronization (operates at the second subharmonic of the pulse repetition rate) and a system of two feedback loops (Fig. 3). The laser system employs two distinct modulators. The first modulator is used for synchronization with an external device. The second modulator is responsible for implementation of the nonlinear dynamics. While the first modulator could be acousto-optic, its operational frequency is typically limited to hundreds of MHz.

The selection of optimal parameters for the chaotic generator control scheme requires investigation of the dynamics for various values of u_0. Let us consider nonlinear dynamics of a laser for generation of multi-gigahertz chaotic pulse sequences (Fig. 4). It was shown earlier that by choosing the delay of negative optoelectronic inertial feedback it is possible to organize a harmonic self-synchronization mode [18] with a large number of pulses m. In order to derive a discrete map that describes the pulse energy evolution from pass to pass of a laser cavity, we assume that stable equidistant laser pulses exist and that their temporal width is short compared to the interpulse interval. Furthermore, we assume that the effects of pulse elongation and shortening can be neglected for the purposes of describing the energy dynamics on a per-pass basis. Thus, the evolution of the pulse energy from one

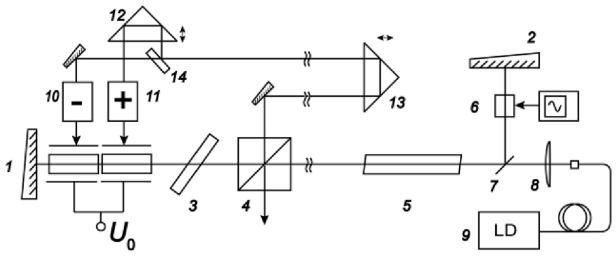

Fig. 3. Schematic diagram of a laser under consideration. 1, 2 resonator mirrors, 3 polarizer, 4, 14 beam splitters, 5 laser active medium, 6 high-frequency (HF) modulator, 7 dichroic mirror, 8 focusing optics, 9 laser diode module, 10 negative feedback loop control circuit, 11 positive feedback loop control circuit, 12, 13 variable delay feedback prisms.

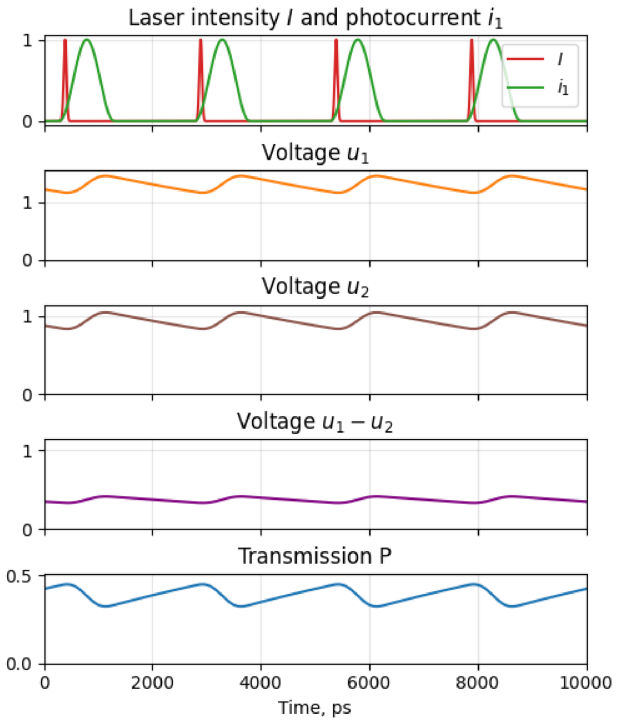

Fig. 4. Dynamics of laser intensity and modulator control signals in the regime of self-mode-locking with four laser pulses in the laser cavity. Resonator length T_r = 10 ns. The current i_{d1} is normalized by its maximum value and thus coincides with current i_{d2}, voltage is normalized by half-wave voltage $u_{\lambda/2}$.

round trip to the next is governed by two primary factors.

First, the pulse is amplified in the active medium and experiences all linear, non-saturable losses in the resonator. The total net gain per pass incorporates the amplification in the active medium, as well as all fixed losses, including the transmission of the intracavity beam splitter and other passive elements.

Second, the pulse energy is subsequently multiplied by the transmission of the electro-optic modulator P, which is a nonlinear function of the control signal. In case of harmonic mode-locking, the control voltage u_1 is determined by the energies of the light pulses that circulate in the laser cavity taking into account the decay of the signal, namely an infinite sum with decay coefficient $e^{-T_r/mRC}$.

The second voltage u_2 is the same sum but taken with relative sensitivity equal to the decay coefficient and delayed by one interpulse interval T_r/m [17].

This results in cancelling out the terms of infinite sum. Therefore, the control signal u depends only on the energy of the pulse on the previous round trip x_n. To simplify the resulting equation and eliminate the feedback sensitivity coefficient from the mapping, the pulse energy x_n is normalized by

this very coefficient. Combining these effects, the discrete mapping for the normalized pulse energy x_{n+1} on the $(n+1)$-th round trip is given by:

$$x_{n+1}=\frac{rx_n\cos^2\left(\frac{\pi}{2}(x_n+u_0)\right)}{\cos^2\left(\frac{\pi}{2}u_0\right)}. \tag{3}$$

Here u_0 represents the constant bias voltage applied to the electro-optic modulator (in the units of half-wave voltage $u_{\lambda/2}$), while r denotes the round-trip gain in the units of lasing threshold. To make comparison of map (3) to the logistic map clear, we use the same notation of normalized energy x_n as in the logistic map:

$$x_{n+1}=rx_n\,(1-x_n). \tag{4}$$

However, to obtain the same amplification in the absence of feedback signal (with $u = 0$), we also normalize the right side of (3) by initial value of $P_0 = \cos^2(u_0\pi/2)$. In this context, the dimensionless parameter r is defined as the total round-trip gain normalized by the lasing threshold condition.

Study of the properties of map (3) will allow us to identify the features of the nonlinear dynamics of multigigahertz solid-state lasers the chaotic generator. To the best of our knowledge, map (3), has not been previously investigated.

3. Map analysis

3.1. Stationary point

Stationary point (or fixed point) of a map is a value of x that remains unchanged after applying the map. Such values can be found by solving the equation $x_p = f(x_p)$. The stationary point of a map (3) is not unique. Equation

$$1/r=\cos^2\left(\frac{\pi(x_p+u_0)}{2}\right)/\cos^2\left(\frac{\pi u_0}{2}\right), \tag{5}$$

when solved for x_p, gives an infinite number of solutions due to periodic nature of cosine function. Solutions can be expressed as follows:

$$x_p=\pm 2/\pi\arccos\left(\pm\cos\left(\frac{\pi u_0}{2}\right)/\sqrt{r}\right)-u_0+4n, n=0,1,2\ldots \tag{6}$$

The fractal nature of map (3) will be considered in the future but is beyond the scope of this paper. Here we consider first positive and zero solution and investigate their stability by calculating multipliers in Sec. 3.3.

3.2. Lyapunov exponents

Being one-dimensional recurrence relation, map (3) allows calculating its Lyapunov exponents using the explicit form of derivative of the right side $f'(x_n)$:

$$\lambda=\frac{1}{n}\sum_{i=0}^{n-1}\ln\left|f'(x_i)\right|, \tag{7}$$

where $x_{(n+1)} = f(x_n)$. For map (3), the derivative equals

$$f'_x=r\frac{\cos\frac{\pi(x+u_0)}{2}}{\cos^2\left(\frac{\pi u_0}{2}\right)}\left(\cos\frac{\pi(x+u_0)}{2}-\pi x\sin\frac{\pi(x+u_0)}{2}\right). \tag{8}$$

For calculation procedure implementation we used the approach described in Ref. [20].

3.3. Stability of stationary point

Using the derivative (6) and the equation from [21]

$$\sum_n\frac{d_n|_{x_p}}{\mu^{n+1}}=1 \tag{9}$$

we can calculate the multipliers μ and then find the region where $|\mu| < 1$ that corresponds to the stability region of map (3).

$$\frac{d_0|_{x_p}}{\mu}=1 \tag{10}$$

$$\mu=d_0|_{x_p} \tag{11}$$

$$\mu=1-\frac{2\left(\arccos\left(\frac{\cos\left(\frac{\pi u_0}{2}\right)}{\sqrt{r}}\right)-\frac{\pi u_0}{2}\right)\sqrt{r-\cos^2\left(\frac{\pi u_0}{2}\right)}}{\cos\left(\frac{\pi u_0}{2}\right)}. \tag{12}$$

Graphs of (12) for several values of u_0 are shown in Fig. 5. By substitution of $\mu = -1$ into (12) we can obtain the upper boundary of stability region which is explicitly defined by the following formula:

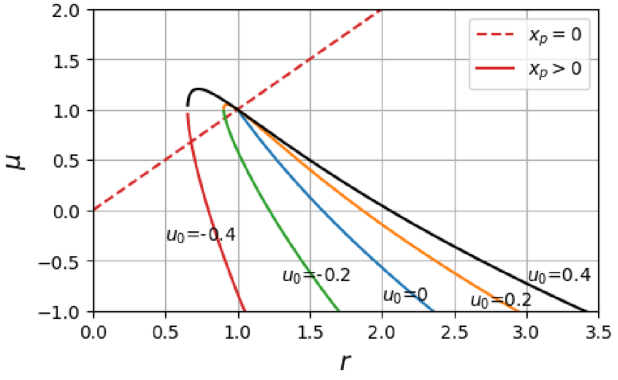

Fig. 5. Values of multipliers (12) vs gain level r at different values of u_0.

$$u_0 = \frac{2}{\pi}\left(\arccos\frac{\cos\left(\frac{\pi u_0}{2}\right)}{\sqrt{r}} - \frac{\cos\left(\frac{\pi u_0}{2}\right)}{\sqrt{r-\cos^2\left(\frac{\pi u_0}{2}\right)}}\right). \quad (13)$$

Substitution of $\mu = 1$ into (12) gives the lower boundary of the stability region:

$$u_0 = \frac{2}{\pi}\arccos\frac{\cos\left(\frac{\pi u_0}{2}\right)}{\sqrt{r}}. \quad (14)$$

While discrete mapping analysis provides valuable insights, it cannot assess the duration of ultrashort pulses or examine their establishment process. Therefore, we conducted numerical simulations to study these aspects.

4. Simulation of laser dynamics with picosecond resolution

The nonlinear dynamics regimes were investigated through numerical simulations based on proven methodologies. The model was introduced in detail in Ref. [18] and accurately describes the results of previous experiments: stationary and complex dynamics in solid-state lasers, including correct prediction of pulse width [22,23] and nonlinear dynamics scenarios [24]. It is based on tracing the field evolution in a laser cavity, taking into account intracavity elements' action. Starting from roundtrip $K = 0$, the spontaneous emission noise N is added to the laser radiation field at each round-trip. We can describe the amplitude transformation from round-trip K to round-trip $(K + 1)$ as

$$A_{K+1}(t) = (1-S)\sqrt{P(t)}\,\frac{exp(g)}{2\sqrt{\pi}\tau_a\sqrt{g}}\int_{-\infty}^{+\infty} A_K(t')\times \times \exp\left[-\left(\frac{t-t'-\tau_a g}{2\tau_a\sqrt{g}}\right)^2\right]dt' + N_K(t). \quad (15)$$

Here g is gain coefficient of active medium at the central wavelength, $\tau_a = (\pi\Delta\nu_L)^{-1}$ and $\Delta\nu_L$ is the active medium gain linewidth. The convolution term in (15) determines the laser pulse elongation, while the shape of $P(t)$ in the vicinity of its maximum determines the pulse shortening. By shifting the feedback delay, the behavior of $P(t)$ at the time interval of T_r can be adjusted towards the appearance of several maxima and thus for the generation of several laser pulses.

For each round-trip K, the laser intensity $I(t)$ is computed from the field amplitude given by Eq. (15). This intensity profile is then used to determine the photodiode currents $i_{d1}(t)$ and $i_{d2}(t)$. Subsequently, the control voltages $u_1(t)$ and $u_2(t)$ are obtained by numerically solving the differential Eqs. (1) and (2). Finally, these voltages define the instantaneous transmission of the electro-optic modulator, $P(t)$, over the time interval $t \in [K\cdot T_r,(K+1)\cdot T_r)$. This computational cycle is performed with a high temporal resolution of 0.1–0.05 ps. In this simulation, we use the value of $R_1C_1 = R_2C_2 = 3T_r/m$, which, similarly to other numerical simulations and experiments [16], allows for stable generation of light pulses and is convenient for comparison and investigation over a wide gain range. For the sake of comparison with map (3), we present simulation results versus the value of r in the units of lasing threshold: $r = \cos^2(u_0\pi/2)\cdot(1-S)^2e^{2g}$ [18,19]. The other parameters used, including the delays and photodiode response times, were the same as in Ref. [17]. A representative result of this procedure, showing the temporal dynamics of these key quantities, is presented in Fig. 4. From these data, the total radiation energy per round-trip, E, and the duration of the most intense spike, τ_L, are calculated at each step. The calculation for a given parameter set is computationally intensive, requiring from several minutes to approximately 24 h on a standard Intel PC (3.3 GHz, 3.25 GB RAM).

5. Results and discussion

The calculation of the bounded nonlinear dynamics region was carried out through 10^6 iterations of map (3) with progressively increasing gain coefficient r. Diagrams for $u_0 = -0.45$, -0.3, 0, 0.5 and 0.9 are shown for example in Fig. 6 and clearly show that the set of dynamical regimes is not affected by u_0 change but gain level shift significantly. Note that, compared to the logistic map (4), all realizations of map (3) have a wider chaotic region that includes a pronounced period 2 window. The values of r at which the window occurs can be calculated by solving the equation

$$x = f(f(x)), \quad (16)$$

where $f(x)$ is the right-hand side of map (3). This equation requires numerical solving and stability analysis of the obtained solutions. In this paper we focus on chaotic threshold. Fig. 7 shows that chaos with positive Lyapunov exponent starts above the period 3 window. We plot the period 3 points together with boundaries of stability region in Fig. 8 obtained from analytical consideration, direct map calculation and numerical simulation accounting for fine temporal structure. The results obtained with all methods are in good correspondence. However, for 10 GHz dynamics, boundary values

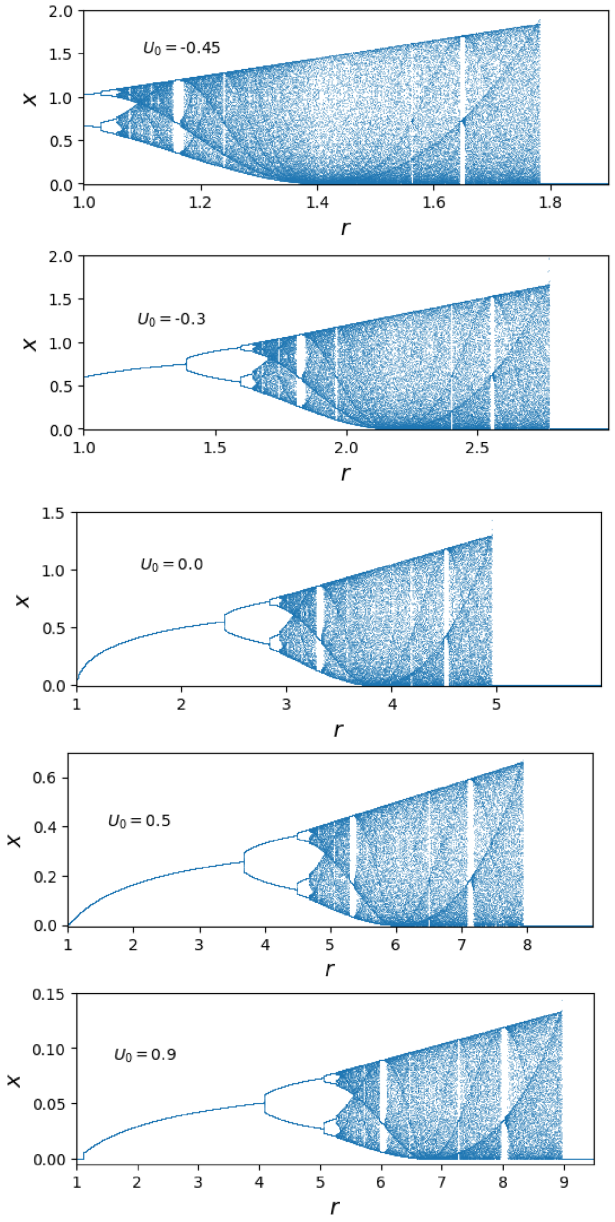

Fig. 6. Phase-parametric diagrams of map (3).

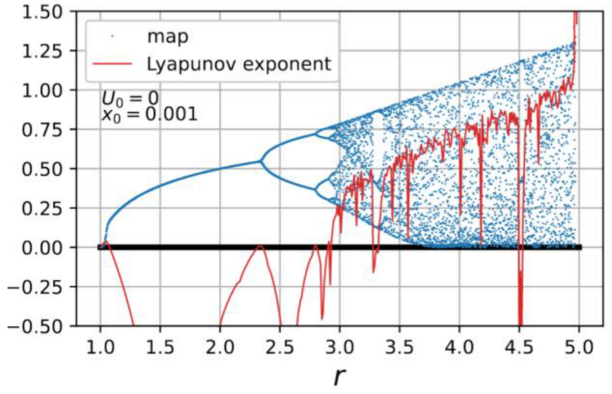

Fig. 7. Lyapunov exponents of map (3) and its dynamics for $u_0 = 0$.

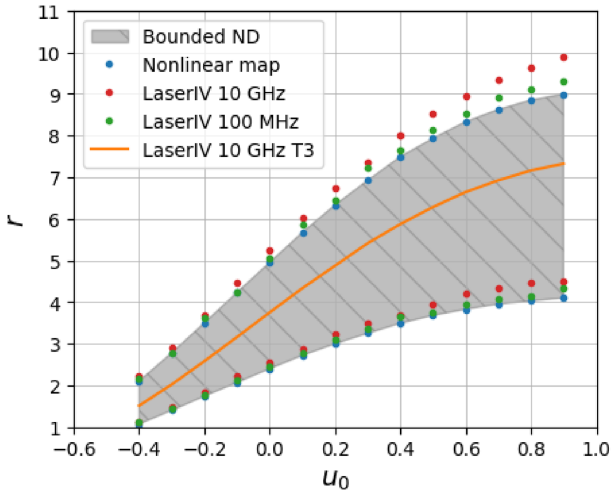

Fig. 8. Calculated minimum and maximum gain levels for nonlinear dynamics implementation obtained through: 1) nonlinear mapping, 2) LaserIV simulations at 10 GHz pulse repetition frequency, and 3) LaserIV simulations at 100 MHz. The period-3 regime is marked by the solid line, with the shaded region corresponding to bounded nonlinear dynamics.

obtained from high-resolution simulation are higher.

Fig. 8 presents the main result of this paper: chaotic threshold significantly decreases when bias voltage u_0 is decreased. To identify the limiting factors, we determined the ranges of control voltages u_1 and u_2 applied to the modulator crystals. The values are shown in Table 1. Furthermore, in Fig. 9 is shown the corresponding amplification on laser active medium. It was obtained taking into

Table 1. Values of control voltages u_1 and u_2 (normalized by half-wave voltage $u_{\lambda/2}$) and gain levels.

u_0	u_1	u_2	r	AM gain
0.5	0.88–1.05	0.63–0.75	3.96	7.92
	0.35–2.15	0.25–1.54	8.52	17.04
0.0	1.86–2.25	1.34–1.61	2.55	2.55
	0.43–4.09	0.31–2.93	5.25	5.25
-0.3	2.54–3.07	1.82–2.20	1.47	1.85
	0.53–5.17	0.38–3.70	2.92	3.68

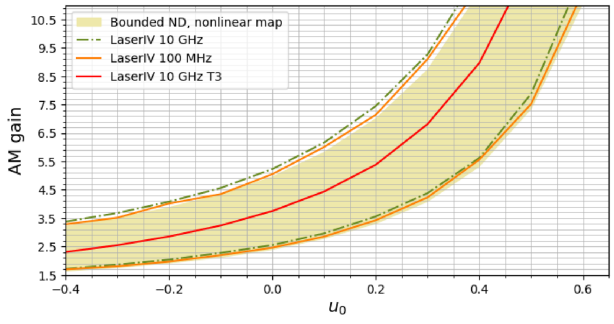

Fig. 9. Active medium amplification levels versus modulator bias voltage u_0 (the notation on legend corresponds to that used in Fig. 8).

account the initial value of modulator transmission $\cos^2(\pi u_0/2u_{\lambda/2})$. Since the control voltage amplitudes increase significantly when u_0 shifts toward negative values, the value of $u_0 = 0$ can be considered optimal for chaotic generator implementation. In this case, only a low-voltage modulator is required, which can be controlled using a mesastructure as experimentally demonstrated in Ref. [22].

Numerical simulation has proven that lowering the chaotic threshold is possible by changing the value of bias voltage in a wide range of pulse repetition frequencies. The build-up process is not longer than 1000 round-trips of the laser resonator which makes the laser simple to operate in a pulsed repetitive mode. The period 3 regime, a key precursor to chaos, is preserved within a significant delay window of 10031–10062 ps (for 10 GHz repetition rate). This demonstrates that the model's predictions are not critically sensitive to exact parameter matching, which is a positive indicator for experimental realizability.

Thus the proposed laser is an attractive platform for further chaotic sources development. The performed analysis is a major step towards reliable high-repetition-rate laser sources. It allows us to estimate the acceptable range active medium amplification.

Our findings yield three key practical advantages: 1) they enable the development of specific recommendations for optimal control parameter selection, 2) significantly facilitate experimental realization of the system, and 3) expand potential applications for chaotic generators. Particularly, the identified operating conditions (zero bias voltage with gain threshold $\leq$1.8) establish a practical foundation for implementing chaotic lasers using low-gain active media, overcoming previous implementation challenges. The combined control approach demonstrated in this work provides a reliable pathway for developing compact, energy-efficient chaotic laser systems. We believe that they will find application in broadband data scrambling using a chaotic masking scheme, physical random number generation and sensing applications.

6. Conclusion

Based on the study of a new type of point mapping, which describes the nonlinear dynamics of a chaotic laser generating multi-gigahertz sequences of equally spaced pulses with a chaotic amplitude distribution, the role of the constant bias of a two-section modulator is determined.

Our systematic investigation of bias voltage effects demonstrates that polarity reversal and the selection of a zero bias voltage significantly reduce the operating gain threshold while maintaining system controllability. The results reveal that the chaotic threshold can be effectively manipulated through modulator bias voltage, with the negative polarity region requiring gain levels not exceeding 1.8. Through comprehensive analysis of dynamics, we have established specific photodiode requirements for the control system and determined that zero bias voltage represents the optimal condition when considering both threshold reduction as well as achievable control signal amplitudes.

Ethics information

The manuscript does not contain any studies involving human participants or animals that require ethical approval.

Funding

This research did not receive any specific grant from funding agencies in the public, commercial, or non-profit sectors.

Conflicts of interest

The authors declare no conflict of interest.

Acknowledgements

The authors express their gratitude to Yu. V. Shabalin, V.A. Petukhov and V.G. Tunkin for useful discussions.

References

[1] H. Gibbs, Optical Bistability: Controlling Light with Light, Elsevier. 2012.
[2] G.G. Akchurin, L.A. Melnikov, Laser Noise Generator, 1988. Patent No. 1441215 (USSR).
[3] F.T. Arecchi, W. Gadomski, R. Meucci, Generation of chaotic dynamics by feedback on a laser, Phys. Rev. A 34 (1986) 1617–1620, https://doi.org/10.1103/PhysRevA.34.1617.
[4] E.V. Grigor'eva, S.A. Kashchenko, N.A. Loĭko, A.M. Samson, Multistability and chaos in a negative-feedback laser, Sov. J. Quantum Electron. 20 (1990) 938–943, https://doi.org/10.1070/QE1990v020n08ABEH007316.
[5] A. Locquet, Routes to chaos of a semiconductor laser subjected to external optical feedback: a review, Photonics 7 (2020) 22, https://doi.org/10.3390/photonics7010022.
[6] S.-L. Yan, Period-control and chaos-anti-control of a semiconductor laser using the twisted fiber, Chin. Phys. B 25 (2016) 090504, https://doi.org/10.1088/1674-1056/25/9/090504.
[7] J. Jani, Unveiling chaos in semiconductor lasers: a simulation-based study using vicente equations, Int. J. Appl. Phys. Eng. 3 (2024) 38–42, https://doi.org/10.37394/232030.2024.3.6.
[8] M. Sciamanna, K.A. Shore, Physics and applications of laser diode chaos, Nat. Photonics 9 (2015) 151–162, https://doi.org/10.1038/nphoton.2014.326.
[9] Y. Wang, Z. Wu, B. Li, J. Chen, L. Shen, H. Yang, Y. Feng, X. Chen, M. Li, Hybrid integrated optical chaos circuits with

optoelectronic feedback, Opt. Express 32 (2024) 15923–15935, https://doi.org/10.1364/OE.515058.
[10] C.M. Kacher, H. Klima, K.W. Kratky, Suppressive influence of periodic and chaotic laser light on cancer cells, Int. J. Model. Ident. Control 5 (2008) 214–220, https://doi.org/10.1504/IJMIC.2008.023124.
[11] A.S. Dmitriev, A.I. Panas, S.O. Starkov, Yu.V. Andreev, L.V. Kuzmin, B.E. Kyarginsky, N.A. Maksimov, Method for Data Transmission by Means of Chaotic Signals, 2000. Patent RU2185032C2 (Russian Federation).
[12] P. Colet, R. Roy, Digital communication with synchronized chaotic lasers, Opt. Lett. 19 (1994) 2056–2058, https://doi.org/10.1364/OL.19.002056.
[13] L. Larger, J.-P. Goedgebuer, Chaotic oscillators for secure optical communications, C. R. Phys. 5 (2004) 609–615, https://doi.org/10.1016/j.crhy.2004.05.004.
[14] M. Suneel, Electronic circuit realization of the logistic map for secure communications, Sadhana 31 (2006) 69–78, https://doi.org/10.1007/bf02703801.
[15] N.K. Pareek, V. Patidar, K.K. Sud, Cryptography using multiple one-dimensional chaotic maps, Phys. Lett. A 309 (2003) 75–82, https://doi.org/10.1016/S0375-9601(03)00122-1.
[16] M.V. Gorbunkov, Y.Y. Maslova, O.I. Chaban, Y.V. Shabalin, Period doubling cascade and deterministic chaos in a laser self-mode-locked by the combination of inertial negative and positive feedbacks, Bull. Lebedev Phys. Inst. 36 (2009) 150–156, https://doi.org/10.3103/S1068335609050054.
[17] M.V. Gorbunkov, Y.Y. Maslova, V.S. Ermakov, Y.A. Sinichkina, Chaotic generator of light pulses with multi-gigahertz repetition rate, Bull. Lebedev Phys. Inst. 52 (2025) 151–158, https://doi.org/10.3103/S1068335624602188.
[18] M.V. Gorbunkov, Y.Y. Maslova, Y.V. Shabalin, V.G. Tunkin, Analysis of self-starting harmonic mode-locking in an electro-optic-feedback laser, IEEE J. Quantum Electron. 57 (2021) 1–8, https://doi.org/10.1109/JQE.2021.3107860.
[19] M.V. Gorbunkov, Y.Y. Maslova, Yu.V. Shabalin, V.G. Tunkin, Variable repetition rate picosecond master oscillator for photoelectron gun, Photonics 9 (2022) 106, https://doi.org/10.3390/photonics9020106.
[20] S. Lynch, Dynamical Systems with Applications Using Python, Birkhäuser, Springer. 2018.
[21] M.V. Gorbunkov, Y.V. Shabalin, Two-loop feedback controlled laser: new possibilities for ultrashort-pulse generation and high-level stabilization, Proc. SPIE 4751 (2002) 463–470, https://doi.org/10.1117/12.475948.
[22] M.V. Gorbunkov, Y.Y. Maslova, V.A. Petukhov, M.A. Semenov, Y.V. Shabalin, A.V. Vinogradov, Submicrosecond regular and chaotic nonlinear dynamics in a pulsed picosecond Nd:YAG laser with millisecond pumping, Appl. Opt. 48 (2009) 2267–2274, https://doi.org/10.1364/AO.48.002267.
[23] M.V. Gorbunkov, Y.Y. Maslova, V.A. Petukhov, M.A. Semenov, Yu V. Shabalin, Generation of a regular sequence of short-pulse microtrains with a discretely varied repetition period, Bull. Lebedev Phys. Inst. 36 (2009) 270–276, https://doi.org/10.3103/S1068335609090048.
[24] M.V. Gorbunkov, Y.Y. Maslova, Y.V. Shabalin, V.G. Tunkin, Dual feedback control in solid state lasers: discrete maps and experiments, J. Phys. Conf. Ser. 692 (2016) 012009, https://doi.org/10.1088/1742-6596/692/1/012009.